Energy Conversion and Management 132 (2017) 261–271

Contents lists available at ScienceDirect

Energy Conversion and Management

journal homepage: www.elsevier.com/locate/enconman

Analytical and numerical investigation on a new compact thermoelectric generator

Tingzhen Ming [a,*], Wei Yang [b], Xiaoming Huang [b], Yongjia Wu [c], Xiaohua Li [d], Jun Liu [e]

[a] School of Civil Engineering and Architecture, Wuhan University of Technology, No. 122, Luoshi Road, Wuhan 430070, China
[b] School of Energy and Power Engineering, Huazhong University of Science and Technology, Wuhan 430074, China
[c] Mechanical Engineering, Virginia Tech, Blacksburg 24061, USA
[d] Department of Mechanical and Energy Engineering, University of North Texas, 1155 Union Circle #311098, Denton, TX 76207, USA
[e] Department of Mechanical and Aerospace Engineering, North Carolina State University, Raleigh, NC 27695, USA

ARTICLE INFO

Article history:
Received 22 August 2016
Received in revised form 1 November 2016
Accepted 18 November 2016
Available online 25 November 2016

Keywords:
Thermoelectric power generator (TEG)
Specific voltage
Specific power
Specific efficiency

ABSTRACT

In order to improve the performance and maximize the efficiency of energy conversion of thermoelectric generator (TEG), a mathematical model to predict the maximum energy conversion efficiency of TEG is developed. Then, a new compact thermoelectric generator (C-TEG) and a dimensional optimized TEG (DO-TEG) are proposed in this article. The compact thermoelectric generator is designed via logical intersection angle selection and layout, thus to improve the electric performance per unit volume. Finally, we compared the output electric performance of C-TEG and traditional thermoelectric generator (T-TEG) and that of DO-TEG under design and off-design conditions via numerical simulations. The results indicate that C-TEG has an excellent electric performance whose voltage, power, and efficiency decrease slightly whereas the output voltage, work, and efficiency compared with that of T-TEG have been significantly improved, with the amplitude increasing with the increase of resistant value of external loads.

1. Introduction

Recently, with the increasing consumption of conventional fuels such as coal, petroleum, and natural gas, the environmental pollution in China has become increasingly severe, which even leads to haze that shall be handled immediately [1–3]. The replacement which is safe, clean, and sustainable is, undoubtedly, a significant measure to save fossil energy and protect the environment. As one of the potential conversions of energy, the thermoelectric technology has attracted worldwide extensive attention, thanks to its safety, noiselessness, sustainability, and the waste heat utilization [4–6]. The thermoelectric generation manages to produce electric potential via the Seebeck effect of semiconductor under the temperature differences [7]. Thermoelectric directly converts heat into electricity, which is broadly applied in the power generation of space satellite [8–11] and waste heat recovery [12–16].

Zhang [17] studied the performance of a thermoelectric generation (TEPG) module and a device designed to convert engine exhaust heat directly into electricity under different operating conditions using a proposed thermoelectric (TE) model. The proposed model was obtained based on the theories such as the first law of thermodynamics, Ohm's law, and nonlinear analytical solution of thermoelectric transport equation. Comparison between the model predictions and the experimental results confirmed that reducing the interfacial electric resistance can enhance the module performance.

The performance of TEG systems significantly depends on the hot side temperature of thermoelectric legs and the temperature difference between the hot side and cold side of the legs. To keep the TEG module working at an optimal condition, Wang et al. [18] proposed an effective solution for enhancing the heat transfer of gas flow in the radial direction to the TEG by means of immersing high temperature heat pipes perpendicularly into the exhaust flow. Conventional heat pipes were radially inserted into a concentric coolant jacket to enhance heat transfer performance at the cold side of TEG modules. Simulation results showed that the closer to the heat source in the pipeline the TEG system is located, the better the power generation that is expected. Moreover, better TEG performance can be expected at a higher engine speed.

Yilbas and Ali [19] investigated the influence of the pin geometric configuration on the TEG performance. In their research, the dimensionless tapering parameter was introduced and its effect on the first and second law efficiencies was examined for various operating conditions including the external load resistance and the temperature ratio. They found that the first and second law

* Corresponding author.
E-mail address: tzming@whut.edu.cn (T. Ming).

http://dx.doi.org/10.1016/j.enconman.2016.11.043
0196-8904/

Nomenclature

A	cross-sectional area of thermoelectric arm, mm^2
A_p	cross-sectional area of p-type, mm^2
A_n	cross-sectional area of n-type, mm^2
A_1	occupied area by T-TEG, mm^2
A_2	occupied area by DO-TEG, mm^2
A_3	occupied area by C-TEG, mm^2
B	distance between p-type and n-type, mm
B_1	T-TEG length, mm
B_2	DO-TEG length, mm
B_3	C-TEG length, mm
D	shape factor, –
d_p, d_n	diameter of p-type, n-type, mm
$d_{p(o)}, d_{n(o)}$	dimensional optimized diameter of p-type, n-type, mm
H_1	T-TEG height, mm
H_2	DO-TEG height, mm
H_3	C-TEG height, mm
I	current, A
K	thermal conductivity of thermoelectric arm, W/K
L	thermoelectric arm height, mm
L_p, L_n	thermoelectric arm height of p-type, n-type, mm
m	the ratio of external load and internal resistance, –
P	output power, W
P'	total output power divided by the total volume/area, W/mm^2
Q_c	heat release of cold end, W
Q_h	heat absorption of hot end, W
R	internal resistance of thermoelectric arm, Ω
R_{load}	external load resistance, Ω
S	shape factor ratio, –
S_{opt}	optimized shape factor ratio, –
T_c	temperature in cold end, K
T_h	temperature in hot end, K
V	output voltage, V
V'	total output voltage divided by the total volume/area, V/mm^2
V_1	occupied volume by T-TEG, mm^3
V_2	occupied volume by DO-TEG, mm^3
V_3	occupied volume by C-TEG, mm^3
W_1	T-TEG width, mm
W_2	DO-TEG width, mm
W_3	C-TEG width, mm

Greek symbols

α	seebeck coefficient, V/K
α_p, α_n	seebeck coefficient of p-type, n-type, V/K
$\bar{\alpha}_p$, $\bar{\alpha}_n$	average seebeck coefficient of p-type, n-type, V/K
λ_p, λ_n	thermal conductivity of p-type, n-type, W/(m·K)
$\bar{\lambda}_p$, $\bar{\lambda}_n$	average thermal conductivity of p-type, n-type, W/(m·K)
ρ_p, ρ_n	resistivity coefficient of p-type, n-type, Ω·m
$\bar{\rho}_p$, $\bar{\rho}_n$	average resistivity coefficient of p-type, n-type, Ω·m
η	conversion efficiency, –
η'	total efficiency divided by the total volume/area, 1/mm^2
θ	angle between P-N type and N-N type

Subscripts

c	cold end of thermoelectric devices
h	hot end of thermoelectric devices
n	n-type of semiconductor
p	p-type of semiconductor
opt	optimized dimensional

efficiencies are significantly influenced by the pin geometry, but the dimensionless tapering parameter maximizing the first and second law efficiencies does not maximize the device output power. Ali et al. [20] thermodynamically analyzed the influence of pin leg geometry on the thermal performance of the TEG. The exponential area variation of pin legs was considered and dimensionless geometric parameter was introduced in the analysis. The influence of dimensionless geometric parameter on efficiency and power output was demonstrated for different temperature ratios and external load resistance ratios. They found that increasing dimensionless geometric parameter can improve the thermal efficiency of the TEG. Sahin and Yilbas [21] investigated the thermodynamic irreversibility and performance characteristics of a TEG. The influence of the external load parameter, the thermal conductivity ratio, the figure of merit, the conductance ratio on the efficiency, the output power, and the entropy generation rate of TEG was predicted for various device operating parameters. They found that the TEG efficiency increases to reach its maximum at the critical value of the output power. Sahin et al. [22] proposed a TEG heated by solar radiation and analyzed the thermal efficiency of the topping cycle and compared with its counterpart without the presence of the thermoelectric elements. Then, they presented a thermodynamic analysis for the efficiency of both the systems with and without a thermoelectric generator and conducted a numerical simulation on the fluid flow and heat transfer in a tube with the presence of thermoelectric elements resembling the solar heating system incorporated in the topping cycle.

Ding et al. [23] proposed a solar pond system with the aid of using TEGs for converting the heat available at lower convective zone into electricity, developed the transient heat transfer model, tested the performance of the thermoelectric module, and analyzed the potential of generating electricity for the solar pond operates in different climates under Koppen climate classification. Later, the effects of heat extraction, climatic variation, temperature polarization, and the conversion efficiency of TEG on the thermal performance and electrical performance of the system were discussed. Shen et al. [24] developed a comprehensive one-dimensional steady theoretical model to analyze the performance of TEGs, in which finite element method and integral averaged Seebeck coefficient are employed to effectively consider the effects of temperature-dependence of thermoelectric materials and Thomson effect respectively. The optimal segments for each case were identified.

Aswal et al. [25] presented an overview on the various aspects of device development, i.e., from the synthesis of high ZT thermoelectric materials to issues and design aspects of the TEG and discussed the various strategies employed to improve ZT. They found that a ZT of >2 has widely been reported by enhancing the power factor and/or reducing the thermal conductivity of the materials.

Dai et al. [26] proposed a hybrid solar hot water and TEG unit using a heat pipe evacuated tube collector with a mini-compound parabolic concentrator, developed a mathematical model regarding the TEG unit, and investigated how to convert excess solar heat into electricity more effectively. They found that the mini-compound parabolic concentrator can significantly improve the electrical efficiency and the TEG could make the best use of excess solar heat when the optimal thermal conductance is determined.

Recently, many new aspects have been mentioned to improve the performance of TEGs, such as: hybrid TEG systems [27–33], segmented TEG systems [34–37], optimization of the design of TEGs [38–42], thermal stress caused by high temperature differences of TEG [42–49], and heat transfer enhancement of the TEGs [25,27,50–59]. Very detailed potential applications of TEGs and methods on how to improve the TEG performance can be found by the review publications [60,61].

However, the study on how to improve the output performance of thermoelectric device with smaller dimensions needs to go further. When applying the TEG to the fields like aerospace or industry, we should take the dual function between its size and voltage, power, or efficiency, hence, maximizing the energy utilization efficiency in the minimal space. Generally speaking, previous studies have adopted traditional inline P-N arrangement for thermoelectric generation module which is plausible but a waste of space consumption, due to its huge size. Therefore, the study in this article adopted a cylindrical thermoelectric couple based upon the traditional prototype, conducted theoretical derivation towards the structural design of thermoelectric couple, and established a physical-mathematical model of the compact thermoelectric device and a dimensional optimization equation for the efficiency maximization. Meanwhile, the ANSYS was used to conduct the calculation and verification of numerical simulation, which in this paper analyzed the electric performance of three thermoelectric devices of different structures, so as to provide theoretical references for the designing of new thermoelectric generation modules.

2. Theoretical analysis

2.1. Maximized efficiency

The efficiency of a thermoelectric generator (TEG) could be defined as the ratio between the electric output power and the heat absorbed at its hot-end.

$$\eta = \frac{P}{Q_h} \tag{1}$$

where η, P, Q_h are the conversion efficiency from heat to electricity, the electric output power, and the heat absorbed at the hot-end, respectively.

The heat fluxes on the cold- and hot- ends of the thermocouple [42] are:

$$Q_h = \alpha T_h I - \frac{1}{2} I^2 R + K(T_h - T_c) \tag{2}$$

$$Q_c = \alpha T_c I + \frac{1}{2} I^2 R + K(T_h - T_c) \tag{3}$$

where Q_c is the heat flux discharged at the cold-end; α is Seebeck Coefficient of the thermoelectric material; T_h and T_c are the temperature at the hot- and cold- ends; R and K are respectively the electrical resistivity and the thermal conductance of the thermoelectric generator.

The current I [42]could be described as:

$$I = \frac{\alpha(T_h - T_c)}{R + R_{load}} \tag{4}$$

where R_{load} is the external load resistance. The energy consumed at the external load could be:

$$P = I^2 R_{\text{load}} = \frac{\alpha^2 (T_h - T_c)^2}{(R + R_{load})^2} R_{load} \tag{5}$$

if $R_{load} = mR$, substituting Eqs. (2) and (5) in Eq. (1), the efficiency is:

$$\eta = \frac{I^2 R_{load}}{\alpha T_h I - \frac{1}{2} I^2 R + K(T_h - T_c)} = \frac{T_h - T_c}{T_h} \cdot \frac{\frac{m}{m+1}}{1 + \frac{KR}{\alpha^2}\frac{m+1}{T_h} - \frac{1}{2}\frac{T_h - T_c}{T_h}\frac{1}{m+1}} \tag{6}$$

Seen from Eq. (6), the efficiency of the thermoelectric generator depends on three kinds of factors, namely, the temperatures at the cold- and hot- ends, the external electric resistance, and the physical parameter of thermoelectric materials.

The Z value of thermoelectric material could be demonstrated as follow:

$$Z = \frac{\alpha^2}{KR} \tag{7}$$

α is the Seebeck coefficient of thermoelectric p-n pair:

$$\alpha = \bar{\alpha}_p - \bar{\alpha}_n \tag{8}$$

where $\bar{\alpha}_p$ and $\bar{\alpha}_n$ are the mean Seebeck coefficient of p-type and n-type legs which, when the physical parameter of thermoelectric materials varies with temperature, could be derived from the integral formulas below:

$$\bar{\alpha}_p = \frac{\int_{T_h}^{T_c} \alpha_p(T) dT}{T_h - T_c} \tag{9}$$

$$\bar{\alpha}_n = \frac{\int_{T_h}^{T_c} \alpha_n(T) dT}{T_h - T_c} \tag{10}$$

The heat conductance K of the thermoelectric pair can be:

$$K = \frac{\bar{\lambda}_p A_p}{L_p} + \frac{\bar{\lambda}_n A_n}{L_n} \tag{11}$$

where $\bar{\lambda}_p$, $\bar{\lambda}_n$ are the mean thermal conductivities of p-type and n-type materials, respectively:

$$\bar{\lambda}_p = \frac{\int_{T_h}^{T_c} \lambda_p(T) dT}{T_h - T_c} \tag{12}$$

$$\bar{\lambda}_n = \frac{\int_{T_h}^{T_c} \lambda_n(T) dT}{T_h - T_c} \tag{13}$$

The electrical resistivity R of the thermoelectric module can be described according to the electrical property and geometrical dimensions of the thermoelectric pair:

$$R = \frac{\bar{\rho}_p L_p}{A_p} + \frac{\bar{\rho}_n L_n}{A_n} \tag{14}$$

where $\bar{\rho}_p$ and $\bar{\rho}_n$ are the mean resistance coefficients of p and n semiconductors:

$$\bar{\rho}_p = \frac{\int_{T_h}^{T_c} \rho_p(T) dT}{T_h - T_c} \tag{15}$$

$$\bar{\rho}_n = \frac{\int_{T_h}^{T_c} \rho_n(T) dT}{T_h - T_c} \tag{16}$$

In Eq. (6), when the material, the temperature difference, and the resistance of external load of thermoelectric pair are given, the value of KR should be minimized so as to maximize the conversion efficiency.

$$KR = \left(\frac{\lambda_p A_p}{L_p} + \frac{\lambda_n A_n}{L_n}\right)\left(\frac{\rho_p L_p}{A_p} + \frac{\rho_n L_n}{A_n}\right) \tag{17}$$

Here, two parameters D and S are introduced: $D = \frac{L}{A}$ is the shape factor of the leg; $S = \frac{D_n}{D_p}$ is the ratio between shape factors. Then, we can get:

$$KR = \left(\frac{\lambda_p A_p}{L_p} + \frac{\lambda_n A_n}{L_n}\right)\left(\frac{\rho_p L_p}{A_p} + \frac{\rho_n L_n}{A_n}\right) = \lambda_p \rho_p + \lambda_p \rho_n S + \frac{\lambda_n \rho_p}{S} + \lambda_n \rho_n \tag{18}$$

When derivating Eq. (18), we could get the optimal ratio of shape factor which minimizes KR, that is, maximizing the conversion efficiency of thermoelectric generator.

$$S_{opt} = \left(\frac{D_n}{D_p}\right)_{opt} = \sqrt{\frac{\lambda_n \rho_p}{\lambda_p \rho_n}} \tag{19}$$

When substituting Eqs. (18) and (19) into Eq. (6), we could obtain the maximized efficiency:

$$\eta == \frac{T_h - T_c}{T_h} \cdot \frac{\frac{m}{m+1}}{1 + \frac{\lambda_p \rho_p + \lambda_p \rho_n \sqrt{\frac{\lambda_n \rho_p}{\lambda_p \rho_n}} + \frac{\lambda_n \rho_p}{\sqrt{\frac{\lambda_n \rho_p}{\lambda_p \rho_n}}} + \lambda_n \rho_n}{\alpha^2} \frac{m+1}{T_h} - \frac{1}{2} \frac{T_h - T_c}{T_h} \frac{1}{m+1}} \tag{20}$$

From the analysis above, a rational choice of the ratio between shape factors of the thermoelectric generator could optimize the overall efficiency [19].

$$S_{opt} = \left(\frac{D_n}{D_p}\right)_{opt} = \frac{L_n A_p}{L_p A_n} \tag{21}$$

When we get the optimized ratio between shape factors and fix the shape of leg (for example, cylindrical leg) with the lengths of n-type and p-type legs being equal, Eq. (21) can be written as follows:

$$S_{opt} = \frac{A_p}{A_n} = \frac{d_{p(o)}^2}{d_{n(o)}^2} \tag{22}$$

Finally, we can get the optimized diameters of p-type and n-type legs.

2.2. Three configurations of TEG

In order to compare the performance of the new TEG designed according to the above analysis with that of the traditional TEG, we assume that the total volume of the materials used for the cylindrical legs is equal and the height of the legs is constant. Then the area of the TEG will vary with different designs as shown in Fig. 1. Fig. 1(a) is the structure of a traditional TEG (T-TEG) without any optimization. Its cross-sectional area is:

$$A_1 = B_1 W_1 = [5B + 0.5(d_p + d_n)]^2 \tag{23}$$

where B is the center distance between the nearest p-type and n-type legs. B_1 and W_1 are respectively the length and width of the area.

According to the analysis shown in Eqs. (1)–(23), the diameters of optimized p-type and n-type legs are $d_{p(o)}$ and $d_{n(o)}$, respectively. The thermoelectric device with dimensional optimization (DO-TEG) could be obtained, as shown in Fig. 1(b). Its cross sectional area could be:

$$A_2 = B_2 W_2 = [5B + d_{n(o)}]^2 \tag{24}$$

Actually, a compacted thermoelectric generator can be achieved by optimizing the configuration based on the structure of DO-TEG. As shown in Fig. 1(c), we define θ (0–90°) as the intersection angle between the ligature of p-n and that of n-n, then the total area of C-TEG is:

$$A_3 = B_3 W_3 = [11B\cos\theta + 0.5(d_{p(o)} + d_{n(o)})][5B\sin\theta + 0.5(d_{p(o)} + d_{n(o)})] \tag{25}$$

According to Eq. (25), an optimized intersection angle θ could be obtained for a C-TEG. The structural design procedure of a C-TEG could be presented in Fig. 2.

In order to further study the evaluation of the performance of thermoelectric device, the specific efficiency, specific voltage, and specific power output were introduced to represent the efficiency, voltage, and power output per unit area of a single module. A higher value of the specific parameter means a TEG module with higher performance.

$$\eta' = \frac{\eta}{A} \tag{26}$$

$$V' = \frac{V}{A} \tag{27}$$

$$P' = \frac{P}{A} \tag{28}$$

3. Numerical simulation

3.1. Physical model

In this work we established three physical models of T-TEG, DO-TEG, and C-TEG as shown in Fig. 3, each of which includes 18 pairs of p-n leg. The models were all composed by heat trapping layer (ceramics), copper slice, and cylinder electric couples, forming generally a structure of electricity-in-series and heat-in-parallel. Both the difference between C-TEG and T-TEG and the difference between C-TEG and DO-TEG lie in the difference of the internal layout of the thermoelectric module. The p-n junction of C-TEG is the alternative layout between the lines whereas that of T-TEG and DO-TEG is the alternative layout inlines.

Fig. 4 shows the basic dimensions of the three TEGs. The thickness of heat trapping layer is $H_{ceramic}$, whereas that of copper is H_{copper}, with H being the length of thermoelectric couples. The sectional diameter of p-Bi_2Ti_3 leg of the T-TEG is d_p, whereas that of n-Bi_2Ti_3 of the T-TEG is d_p. The sectional diameter of p-Bi_2Ti_3 of the DO-TEG and C-TEG is $d_{p(o)}$, whereas that of n-Bi_2Ti_3 of the DO-TEG and C-TEG is $d_{p(o)}$, with B being the space between p-type and n-type legs. The fundamental dimensions of TEG are listed in the Table 1.

According to the Eqs. (23) and (24), it could be determined that the area occupied by T-TEG is 824 mm^2, and that of DO-TEG is 841 mm^2. Therefore, the area (volume) of DO-TEG is slightly greater than that of T-TEG. As shown in Fig. 5, the area of C-TEG could be represented as the curve varying with the angle, which could be determined via the Eq. (25). Points A and B indicate the area of T-TEG. When the intersection angle θ ranges from 0 to 29.45° and from 57.3° to 90°, the area of C-TEG is smaller than that of T-TEG, and the closer the angle to 0°and 90°, the smaller the area of C-TEG will be, which makes the TEG in this paper a "C-TEG" in the real sense. What should be paid attention to is that, through the comparison between Fig. 1(b) and (c) we could find that when θ = 0° or 90°, the C-TEG would be transformed into DO-TEG. Thus we should maintain the variation interval of θ within the range from 0° to 90°.

Numerical simulation was conducted in this work to analyze the performance of the three TEGs. The temperatures of the hot-end and cold-end are set as 438 K and 298 K, respectively. The external electric resistance is 0.4 Ω (equivalent to the internal

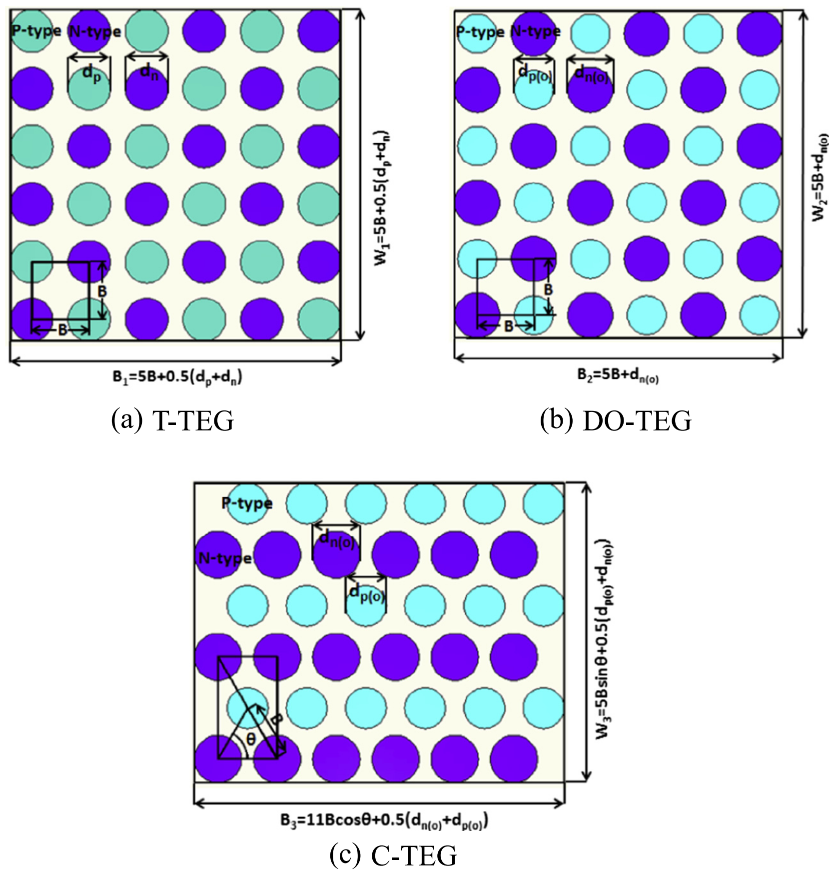

Fig. 1. The layouts of three TEG modules.

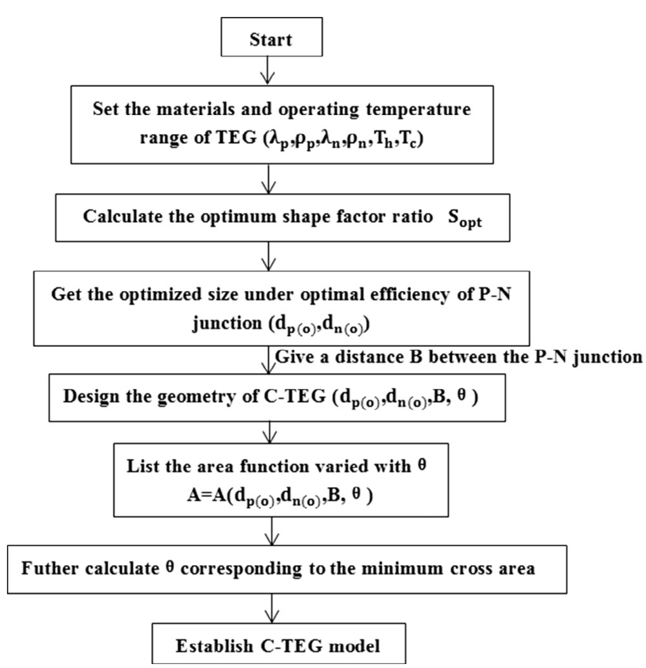

Fig. 2. The design procedure of a C-TEG.

electric resistance), and the efficiency of thermoelectric module is 4.86%, via which, when being translated into specific efficiency, the variation curve could be derived as shown in the Fig. 6. Seen from this figure, the specific efficiency of C-TEG varies with θ, whose tendency goes against that of the area change in Fig. 5. When the efficiency is fixed, with the decrease of area, the variation of θ (ranging from 0° to 29.45° and from 57.3° to 90°) will speed up, accompanied by a sharp increase of specific efficiency of C-TEG. The choice of intersection angle θ could be determined according to the actual circumstances. The study in this paper chose 60° to conduct simulative calculation.

3.2. The physical parameters

According to the theoretical solution from the maximum efficiency, when the material, temperature difference, and external electric resistance of TEG are fixed, the fundamental dimensions could be determined. In this study, Bi_2Te_3 was chosen to be the thermoelectric material. Under the pre-established working condition, the hot-end was given the fixed temperature 438 K, the cold junction the fixed temperature 298 K, with the external temperature 293 K. The physical parameter thereof is presented in Fig. 7 and Table 2.

3.3. Validation of the theoretical model

To validate the correctness of the theoretical model shown above, we conducted a comparison between numerical simulation results and the analytical result for the maximum efficiency shown in Eq. (20) in dimensional optimized TEG as shown in Fig. 8. From this Figure, we can see that the variation trend numerical simulation agrees very well with the analytical result. The maximum differentiation of the efficiency between the numerical and analytical results is 2.5% at most, which could be the verification of the accuracy of efficiency equation.

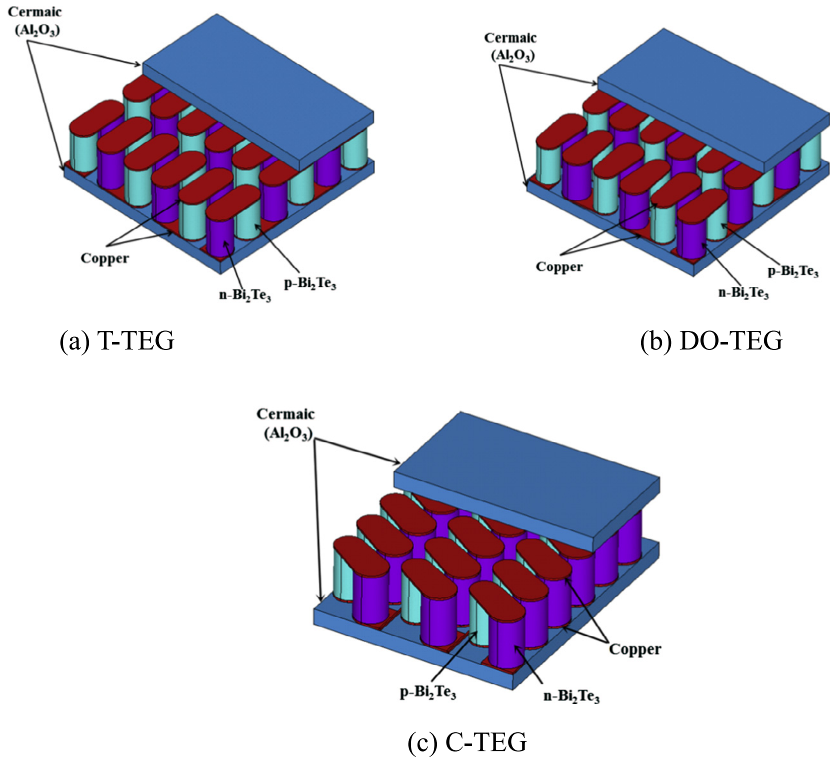

Fig. 3. The structural layout of three TEGs.

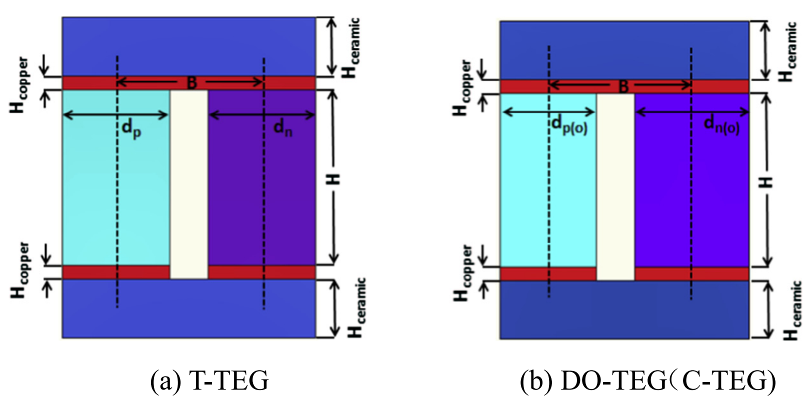

Fig. 4. P-N structural dimension.

Table 1
The structural dimensions of TEG.

The fundamental dimensions	Dimensions
d_p of p-Bi_2Te_3 (mm)	3.7
d_p of n-Bi_2Te_3 (mm)	3.7
$d_{p(o)}$ of p-Bi_2Te_3 (mm)	3.36
$d_{p(o)}$ of n-Bi_2Te_3 (mm)	4
H of p-n legs (mm)	6
The space between p and n legs B (mm)	5
H_{copper} (mm)	0.25
$H_{ceramic}$ (mm)	2
The intersection angle θ (°)	0–29.45° and 57.3–90°

4. Results and discussion

In order to verify the simulation results, the grid independence analysis was completed before the calculation via ANSYS. Under the given boundary conditions, when the internal resistance is 0.4 Ω, the number of grid element is 1,075,545, with 0.47535 V the output voltage, when the number of grid element is 1,164,057, the output voltage is 0.47533 V, and when the number of grid element is 1,409,925, the output voltage is 0.47536 V. The maximum differentiation between output voltage is 0.0063% at most, which could be the verification of the accuracy of simulative results in this study. Thereby, the number of grid element 1,164,057 is selected during the following calculations.

4.1. The simulation under the working conditions

Fig. 9 represents the variation of output voltage with the external electric resistance of three different TEG models. Seen from the figure, for TEGs with 18 pairs of p-n legs structure, the overall output voltage has little difference, because the voltage is mainly determined by the number of thermoelectric pairs if all other conditions are equal. In order to fully consider the generation

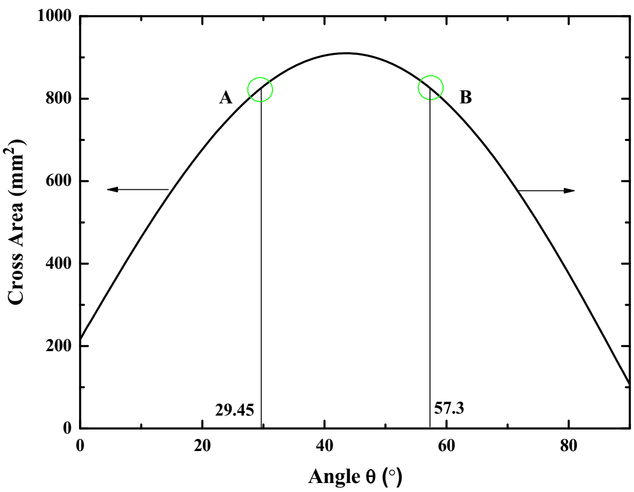

Fig. 5. The area variation of C-TEG with angle.

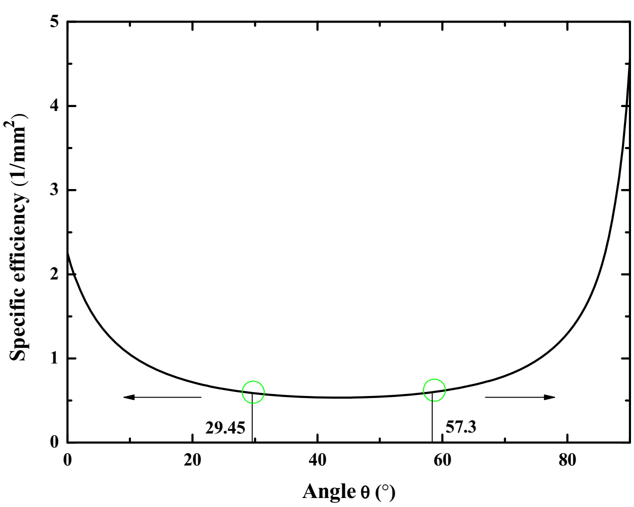

Fig. 6. The variation of specific efficiency of C-TEG with angle.

performance, here the concept of specific voltage was introduced in this study, namely the ratio between the output voltage and the overall dimension of TEG. Since the height of three TEGs is the same, the specific voltage could be defined as the ratio between the output voltage and the cross-sectional area of TEGs, with V/mm^2 the unit. The specific output of C-TEG is generally larger than those of T-TEG and DO-TEG. The reason is that, when the output voltage differs little, the dimension of C-TEG is much smaller than T-TEG and DO-TEG, which is very significant for the power supply in the limited space. Besides, with the increase of load, the increase of specific voltage also speeds up. Compared with T-TEG, the increase rate of DO-TEG is 3.59% when the internal resistance is 0.1 Ω, which increases to 4.63% when the internal resistance is 0.8 Ω.

Fig. 10 indicates the variation of power output with external electric resistance among different TEG structures. It can be seen that the power output of DO-TEG is greater than that of C-TEG, and the power output of C-TEG is slightly greater than that of T-TEG, this is because the output voltage of DO-TEG is slightly larger than the other two. When the external electric resistance is equal to the internal, the above three TEGs (C-TEG, DO-TEG, and T-TEG) have the power output 0.56485 W, 0.55348 W, and 0.55001 W, respectively. At this time, the power output differences of them reach the maximum value.

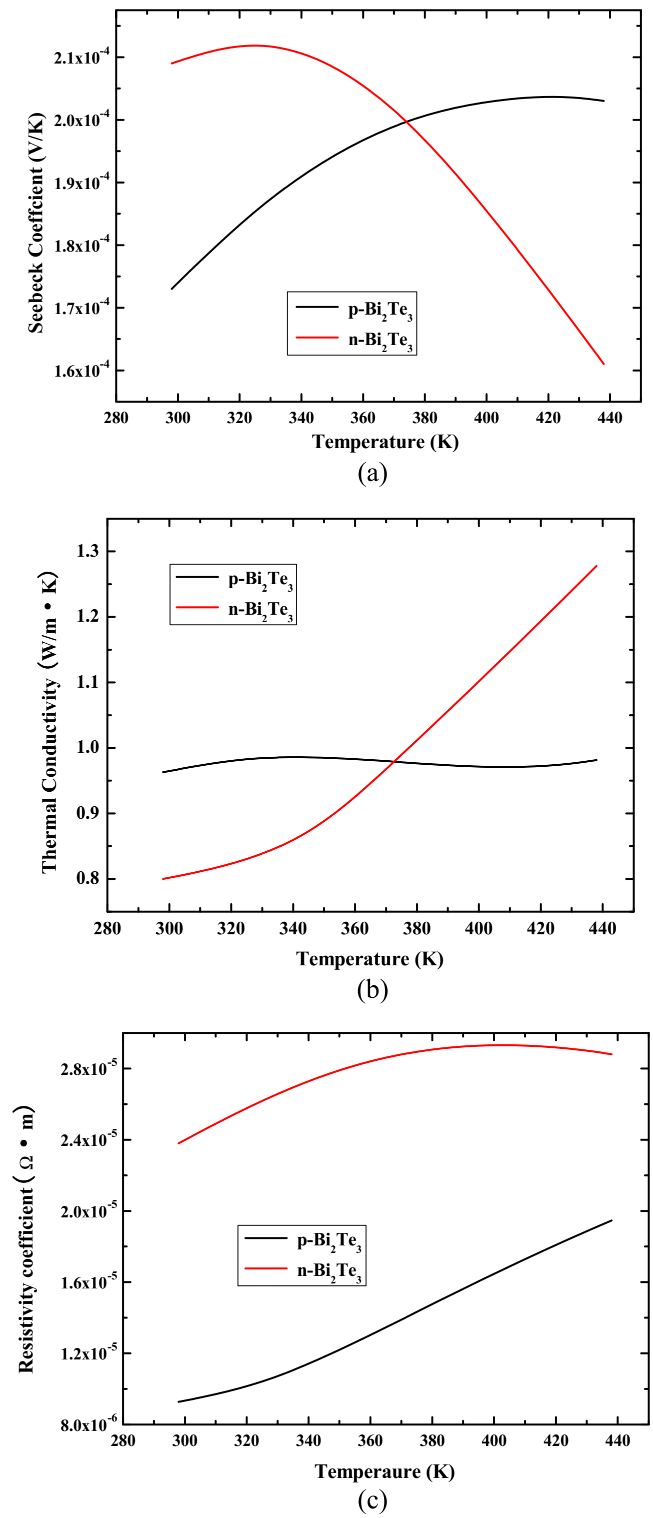

Fig. 7. The variation of the physical parameter of thermoelectric material with temperature [20]: (a) The variation of Seebeck with temperature; (b) The variation of heat conduction coefficient with temperature; (c) The variation of resistance coefficient with temperature.

However, what we should pay attention to is that when comparing the specific power output among those three TEGs as shown in Fig. 9, the performance of C-TEG will be improved. Here, the specific power outputs of T-TEG and DO-TEG are approximately equal, whereas that of C-TEG is slightly higher and increases with

Table 2
The physical parameter of materials.

Material	Conduction coefficient W/(mK)	Resistance coefficient (Ω m)
Copper slice	400	2.5
Heat trapping layer	25	–

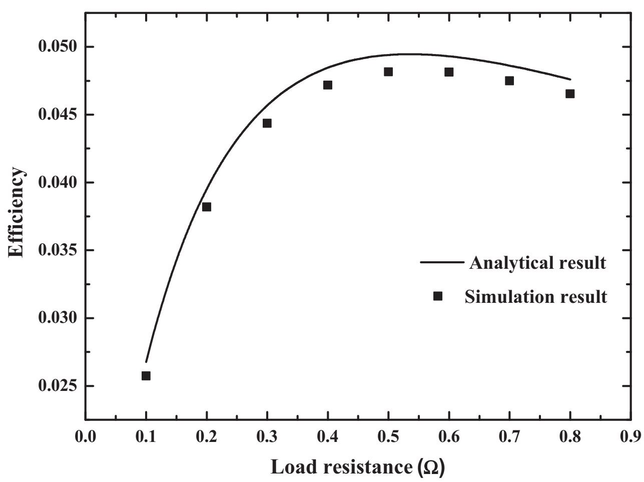

Fig. 8. The validation of efficiency in dimensional optimized TEG.

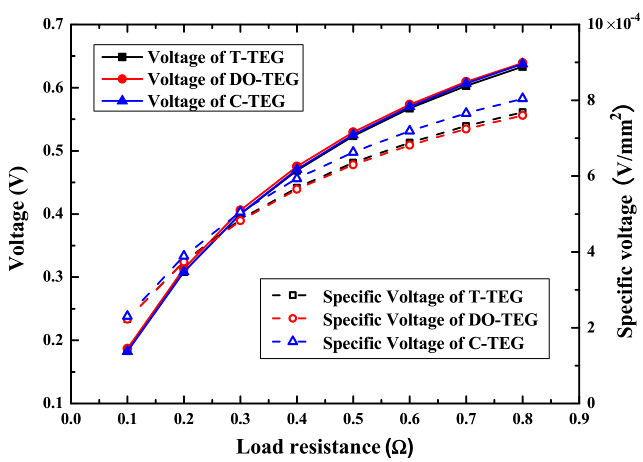

Fig. 9. The variation of output voltage with external electric resistance of different thermoelectric structures.

increasing external electric resistance. When R = 0.1 Ω, the power output of C-TEG is 3.25% higher than T-TEG; when R = 0.8 Ω, the power output of C-TEG is 5.33% higher than T-TEG.

Fig. 11 shows the variation of TEG's energy conversion efficiency with external electric resistance. The efficiency curve has the similar variation tendency with the power output curve. The efficiency of DO-TEG is higher than the other two, which has verified the previous theoretical design. That is, the efficiency of the DO-TEG is the highest, whereas those of T-TEG and C-TEG have not much in difference. Further, with the increase of external electric resistance, the efficiency of DO-TEG also has a rise-fall tendency. The peak point appears where the load resistance is 0.5 Ω, and at this point, the gap of conversion efficiency between DO-TEG and T-TEG is the biggest. Further, the variation of specific efficiency is also on a rise-fall tendency. The specific efficiency of C-TEG is higher than T-TEG and DO-TEG, whose gap becomes

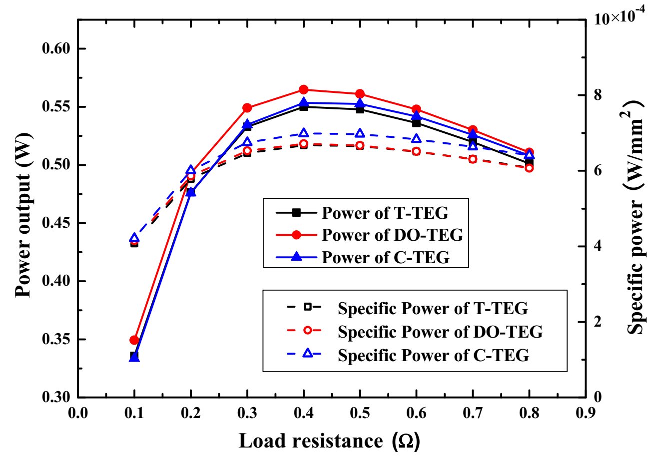

Fig. 10. The variation of power output with external electric resistance of different thermoelectric structures.

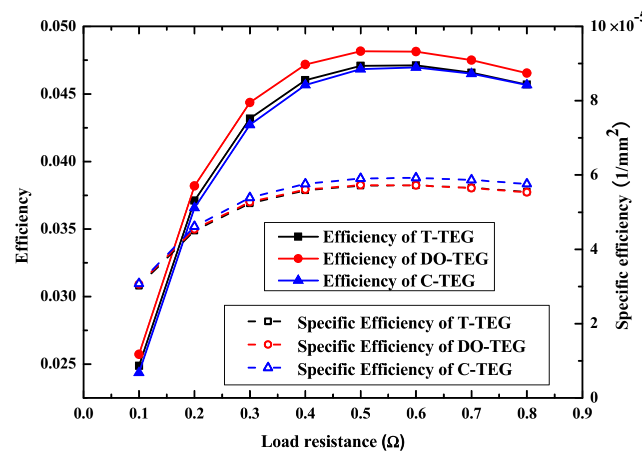

Fig. 11. The efficiency variation of different thermoelectric structures with external electric resistance.

larger with the increase of resistance. When R = 0.1 Ω, the specific efficiency of C-TEG is 3.07498×10^{-5}, and that of T-TEG is 3.01954×10^{-5}, which means the former is 1.84% higher than T-TEG; when R = 0.8 Ω, the specific efficiency of C-TEG is 5.76199×10^{-5}, and that of T-TEG is 5.54648×10^{-5}, which means the efficiency of C-TEG is 3.89% higher than that of T-TEG.

4.2. The simulation results under off-design working conditions

The above analyses of numerical simulation are all based upon the thermoelectric structure under the design working conditions. However, the situations under the off-design working conditions also worth our attention. Thus, when the external electric resistance is 0.4 Ω (the external and the internal resistances are equal), and the temperature at the cold junction is 298 K, the temperature at the hot-end is set to vary with the amplitude of 15 K. Namely, the temperatures at the hot-end are 393 K, 408 K, 423 K, 438 K, 453 K, 468 K, and 483 K, respectively. Under the conditions hereof, the study in this article compared the output performance of the above three thermoelectric structures.

Fig. 12 shows the variation of output voltage of different thermoelectric structures with the temperature at the hot-end. Seen from the curves in this figure, the output voltage has a linear variation with temperature. When the temperature at the hot-end

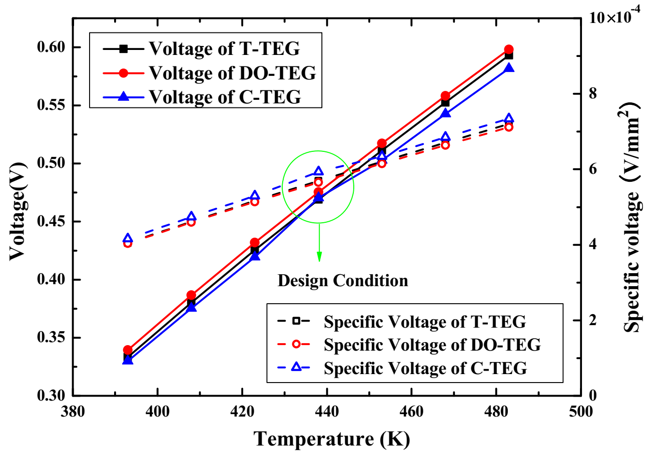

Fig. 12. The variation of output voltage of different thermoelectric structures with the temperature at the hot-end.

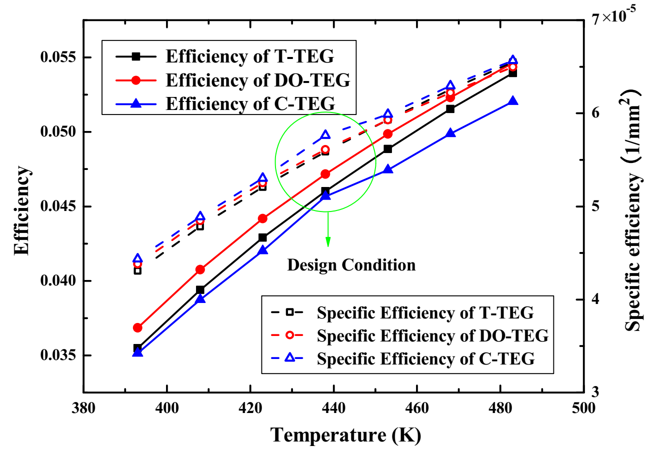

Fig. 14. The efficiency variation of different thermoelectric structures with the temperature at the hot-end.

changes, the output voltage of DO-TEG is slightly higher than those of C-TEG and T-TEG (T_h = 438 K). The disparity of output voltage among three structures is the smallest, which could be regarded as approximate equivalence. In addition, according to the specific voltage output curve, the output of C-TEG is higher than the other two under all working conditions, among which, the disparity reaches the maximum at the critical point of working condition, 4.27%. Apparently, C-TEG could take its better advantages under the design working condition.

Fig. 13 shows the curve of the power output variation of different thermoelectric structures with the temperature at the hot-end. The same to the variation of voltage, the power output of different TEGs rises with that of the temperature at the hot-end, and the increased amplitude of DO-TEG is slightly more than that of the other two structures. At the critical point of design working condition, the disparity among three TEGs reaches the minimum, approximately equal. However, the situation in the specific power output curve is quite the opposite. The simulative results show that, at the point of off-design working condition, the specific power output of three TEGs differs little. At the critical point of design working condition, the C-TEG appears to be more advantageous. Compared with T-TEG, the power output of C-TEG has an increase up to 4.6%.

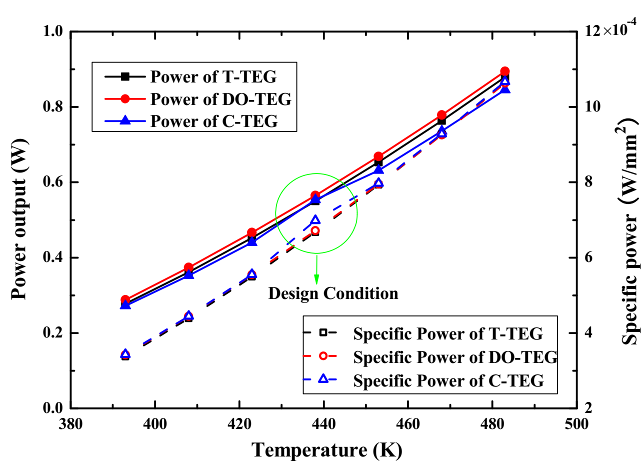

Fig. 13. The power output variation of different thermoelectric structures with the temperature at the hot-end.

Fig. 14 indicates the efficiency variation curve of different thermoelectric structures with the temperature at the hot-end. With the increase of the temperature at the hot-end, the efficiency is on a rising tendency. Here, the efficiency of DO-TEG is generally the best, followed by T-TEG, with the C-TEG the lowest. This is just the result of optimizing the dimensions of the couple. However, at the critical point of design working condition, the efficiency of T-TEG and C-TEG is approximately equal. Yet, in the specific efficiency curve, different tendencies are indicated. That is, the specific efficiency of C-TEG is slightly higher than the other two, within which the disparity between C-TEG and T-TEG under the design working condition reaches 3.2%, the maximum.

5. Conclusions

In allusion to the low electric output performance of T-TEG per unit volume, a new compact TEG design method was advanced in this study to save the space to the uttermost extent and to improve the specific output electric performance, which can provide certain convenience for the application of TEG in the fields such as aerospace and automobile. After designing the thermoelectric model for the maximum efficiency under the corresponding boundary conditions, the following conclusions may be drawn via the numerical simulation of T-TEG, DO-TEG, and C-TEG under the design working conditions and off-design working conditions:

Under the working conditions:

(1) The disparity of output voltage among T-TEG, DO-TEG, and C-TEG differs negligibly. However, the specific voltage of C-TEG is higher than T-TEG and DO-TEG, and the increased amplitude will be on a rise with the increase of the resistance of the external load. When R = 0.8 Ω, the voltage of C-TEG is 4.63% higher than that of T-TEG.
(2) The power output of DO-TEG is higher than that of T-TEG and C-TEG. However, the output specific power of DO-TEG is lower than that of C-TEG whose specific power output is greater than that of T-TEG and DO-TEG and the increased amplitude grows with the increase of external electric resistance. When R = 0.8 Ω, the specific power output is improved by 5.33% in comparison of T-TEG.
(3) The variation of efficiency is similar to that of power output. Namely, the efficiency of DO-TEG is higher than those of T-TEG and C-TEG. When the external electric resistance wanders around 0.5 Ω, the disparity reaches the maximum. Yet, the specific power of C-TEG is higher than those of

T-TEG and DO-TEG, whose increase amplitude grows with the increase of external electric resistance. When R = 0.8 Ω, the specific power of C-TEG is 3.89% higher than that of T-TEG.

Under the off-design working conditions:

(4) The output voltage, power output, and efficiency of DO-TEG are better than those of C-TEG, but the specific output electric performance of C-TEG is better than the other two TEG models. At the critical point of design working condition, the disparity among three structures reaches the maximum, which means that the performance of C-TEG is optimal at the critical point of design working conditions. During the utilization in the actual situation, we could design specific TEG modules according to the external environment.

Author contributions

Tingzhen Ming and Wei Yang contributed equally to the work.

Acknowledgements

This research was supported by the National Natural Science Foundation of China (Nos. 51576077, 51106060), the Scientific Research Foundation of Wuhan University of Technology (No. 40120237), Fundamental Research Funds for the Central Universities (WUT Grant No. 2016IVA029), and the ESI Discipline Promotion Foundation of WUT (No. 35400664).

References

[1] Han F, Xu J, He YJ, Dang HY, Yang X, Meng F. Vertical structure of foggy haze over the Beijing-Tianjin-Hebei area in January 2013. Atmos Environ 2016;139:192–204.
[2] Liu ZR, Wang YS, Hu B, Ji DS, Zhang JK, Wu FK, et al. Source appointment of fine particle number and volume concentration during severe haze pollution in Beijing in January 2013. Environ Sci Pollut Res 2016;23(7):6845–60.
[3] Guo SJ, Chen M. Pollution characteristic of atmospheric carbonyls during one haze event in Nanning, South China. Aeros Air Qual Res 2016;16(5):1143–51.
[4] Venkatasubramanian R, Siivola E, Colpitts T, O'Quinn B. Thin-film thermoelectric devices with high room-temperature figures of merit. Nature 2001;413(6856):597–602.
[5] Heremans JP, Jovovic V, Toberer ES, Saramat A, Kurosaki K, Charoenphakdee A, et al. Enhancement of thermoelectric efficiency in PbTe by distortion of the electronic density of states. Science 2008;321(5888):554–7.
[6] Bell LE. Cooling, heating, generating power, and recovering waste heat with thermoelectric systems. Science 2008;321(5895):1457–61.
[7] Michener WH. Apparatus review – thermoelectric generator. Am J Phys 1961;29(4). 273-&.
[8] Nesbitt JA, Opila EJ, Nathal MV. In situ growth of a Yb_2O_3 layer for sublimation suppression for Yb14MnSb11 thermoelectric material for space power applications. J Electron Mater 2012;41(6):1267–73.
[9] Ezzat MA. State space approach to thermoelectric fluid with fractional order heat transfer. Heat Mass Transfer 2012;48(1):71–82.
[10] O'Brien RC, Ambrosi RM, Bannister NP, Howe SD, Atkinson HV. Safe radioisotope thermoelectric generators and heat sources for space applications. J Nucl Mater 2008;377(3):506–21.
[11] Yang JH, Caillat T. Thermoelectric materials for space and automotive power generation. MRS Bull 2006;31(3):224–9.
[12] Weng CC, Huang MJ. A simulation study of automotive waste heat recovery using a thermoelectric power generator. Int J Therm Sci 2013;71:302–9.
[13] Gou XL, Yang SW, Xiao H, Ou Q. A dynamic model for thermoelectric generator applied in waste heat recovery. Energy 2013;52:201–9.
[14] Shu GQ, Zhao J, Tian H, Liang XY, Wei HQ. Parametric and exergetic analysis of waste heat recovery system based on thermoelectric generator and organic rankine cycle utilizing R123. Energy 2012;45(1):806–16.
[15] Hsu CT, Huang GY, Chu HS, Yu B, Yao DJ. Experiments and simulations on low-temperature waste heat harvesting system by thermoelectric power generators. Appl Energ 2011;88(4):1291–7.
[16] Dai D, Zhou YX, Liu J. Liquid metal based thermoelectric generation system for waste heat recovery. Renew Energ 2011;36(12):3530–6.
[17] Zhang T. New thinking on modeling of thermoelectric devices. Appl Energ 2016;168:65–74.
[18] Wang XZ, Li B, Yan YY, Liu S, Li J. A study on heat transfer enhancement in the radial direction of gas flow for thermoelectric power generation. Appl Therm Eng 2016;102:176–83.
[19] Yilbas BS, Ali H. Thermoelectric generator performance analysis: influence of pin tapering on the first and second law efficiencies. Energ Convers Manage 2015;100:138–46.
[20] Ali H, Sahin AZ, Yilbas BS. Thermodynamic analysis of a thermoelectric power generator in relation to geometric configuration device pins. Energ Convers Manage 2014;78:634–40.
[21] Sahin AZ, Yilbas BS. Thermodynamic irreversibility and performance characteristics of thermoelectric power generator. Energy 2013;55:899–904.
[22] Sahin AZ, Yilbas BS, Shuja SZ, Momin O. Investigation into topping cycle: thermal efficiency with and without presence of thermoelectric generator. Energy 2011;36(7):4048–54.
[23] Ding LC, Akbarzadeh A, Date A. Transient model to predict the performance of thermoelectric generators coupled with solar pond. Energy 2016;103:271–89.
[24] Shen ZG, Wu SY, Xiao L, Yin G. Theoretical modeling of thermoelectric generator with particular emphasis on the effect of side surface heat transfer. Energy 2016;95:367–79.
[25] Aswal DK, Basu R, Singh A. Key issues in development of thermoelectric power generators: high figure-of-merit materials and their highly conducting interfaces with metallic interconnects. Energ Convers Manage 2016;114:50–67.
[26] Dai YJ, Hu HM, Ge TS, Wang RZ, Kjellsen P. Investigation on a mini-CPC hybrid solar thermoelectric generator unit. Renew Energ 2016;92:83–94.
[27] Oshima K, Asano H, Shiraishi Y, Toshima N. Dispersion of carbon nanotubes by poly(Ni-ethenetetrathiolate) for organic thermoelectric hybrid materials. Jpn J Appl Phys 2016;55(2).
[28] Zhao MZ, Zhang HC, Hu ZY, Zhang ZF, Zhang JJ. Performance characteristics of a direct carbon fuel cell/thermoelectric generator hybrid system. Energ Convers Manage 2015;89:683–9.
[29] Mizoshiri M, Mikami M, Ozaki K. Thermal-photovoltaic hybrid solar generator using thin-film thermoelectric modules. Jpn J Appl Phys 2012;51(6).
[30] Chavez-Urbiola EA, Vorobiev YV, Bulat LP. Solar hybrid systems with thermoelectric generators. Sol Energy 2012;86(1):369–78.
[31] Astrain D, Martinez A, Rodriguez A. Improvement of a thermoelectric and vapour compression hybrid refrigerator. Appl Therm Eng 2012;39:140–50.
[32] Miljkovic N, Wang EN. Modeling and optimization of hybrid solar thermoelectric systems with thermosyphons. Sol Energy 2011;85(11):2843–55.
[33] Kim SK, Won BC, Rhi SH, Kim SH, Yoo JH, Jang JC. Thermoelectric power generation system for future hybrid vehicles using hot exhaust gas. J Electron Mater 2011;40(5):778–83.
[34] Tian H, Sun XX, Jia Q, Liang XY, Shu GQ, Wang X. Comparison and parameter optimization of a segmented thermoelectric generator by using the high temperature exhaust of a diesel engine. Energy 2015;84:121–30.
[35] Ming T, Wu Y, Peng C, Tao Y. Thermal analysis on a segmented thermoelectric generator. Energy 2015;80(1):388–99.
[36] Kuznetsov VL, Kuznetsova LA, Kaliazin AE, Rowe DM. High performance functionally graded and segmented Bi2Te3-based materials for thermoelectric power generation. J Mater Sci 2002;37(14):2893–7.
[37] Hadjistassou C, Kyriakides E, Georgiou J. Designing high efficiency segmented thermoelectric generators. Energ Convers Manage 2013;66:165–72.
[38] Brownell E, Hodes M. Optimal design of thermoelectric generators embedded in a thermal resistance network. IEEE Trans Comp Pack Man 2014;4(4):612–21.
[39] Lee H. Optimal design of thermoelectric devices with dimensional analysis. Appl Energ 2013;106:79–88.
[40] Hodes M. Optimal design of thermoelectric refrigerators embedded in a thermal resistance network. IEEE Trans Comp Pack Man 2012;2(3):483–95.
[41] Jang B, Han S, Kim JY. Optimal design for micro-thermoelectric generators using finite element analysis. Microelectron Eng 2011;88(5):775–8.
[42] Al-Merbati AS, Yilbas BS, Sahin AZ. Thermodynamics and thermal stress analysis of thermoelectric power generator: influence of pin geometry on device performance. Appl Therm Eng 2013;50(1):683–92.
[43] Ziabari A, Suhir E, Shakouri A. Minimizing thermally induced interfacial shearing stress in a thermoelectric module with low fractional area coverage. Microelectron J 2014;45(5):547–53.
[44] Sakamoto T, Iida T, Ohno Y, Ishikawa M, Kogo Y, Hirayama N, et al. Stress analysis and output power measurement of an n-Mg2Si thermoelectric power generator with an unconventional structure. J Electron Mater 2014;43(6):1620–9.
[45] Oiler J, Tang R, Ma T, Yu HY. Thermoelectric cool-film shear stress sensor. IEEE Electr Device L 2014;35(7):783–5.
[46] Suhir E, Shakouri A. Predicted thermal stress in a multileg thermoelectric module (TEM) design. J Appl Mech-T ASME 2013;80(2).
[47] Dedi PC, Lee CH, Chien GP, Dong WC, Huang CL, Chen CM, et al. Stress-induced growth of single-crystalline lead telluride nanowires and their thermoelectric transport properties. Appl Phys Lett 2013;103(2).
[48] Ming TZ, Wang QK, Peng KY, Cai Z, Yang W, Wu YJ, et al. The influence of non-uniform high heat flux on thermal stress of thermoelectric power generator. Energies 2015;8(11):12584–602.
[49] Wu YJ, Ming TZ, Li XH, Pan T, Peng KY, Luo XB. Numerical simulations on the temperature gradient and thermal stress of a thermoelectric power generator. Energ Convers Manage 2014;88:915–27.

[50] Suarez F, Nozariasbmarz A, Vashaee D, Ozturk MC. Designing thermoelectric generators for self-powered wearable electronics. Energy Environ Sci 2016;9(6):2099–113.
[51] Soprani S, Haertel JHK, Lazarov BS, Sigmund O, Engelbrecht K. A design approach for integrating thermoelectric devices using topology optimization. Appl Energ 2016;176:49–64.
[52] Shafii MB, Shahmohamadi M, Faegh M, Sadrhosseini H. Examination of a novel solar still equipped with evacuated tube collectors and thermoelectric modules. Desalination 2016;382:21–7.
[53] Remeli MF, Date A, Orr B, Ding LC, Singh B, Affandi NDN, et al. Experimental investigation of combined heat recovery and power generation using a heat pipe assisted thermoelectric generator system. Energ Convers Manage 2016;111:147–57.
[54] Rahbar N, Esfahani JA, Asadi A. An experimental investigation on productivity and performance of a new improved design portable asymmetrical solar still utilizing thermoelectric modules. Energ Convers Manage 2016;118:55–62.
[55] Najjar YSH, Kseibi MM. Heat transfer and performance analysis of thermoelectric stoves. Appl Therm Eng 2016;102:1045–58.
[56] Menon AK, Yee SK. Design of a polymer thermoelectric generator using radial architecture. J Appl Phys 2016;119(5).
[57] Candadai AA, Kumar VP, Barshilia HC. Performance evaluation of a natural convective-cooled concentration solar thermoelectric generator coupled with a spectrally selective high temperature absorber coating. Sol Energy Mater Sol Cells 2016;145:333–41.
[58] Benn SP, Poplaski LM, Faghri A, Bergman TL. Analysis of thermosyphon/heat pipe integration for feasibility of dry cooling for thermoelectric power generation. Appl Therm Eng 2016;104:358–74.
[59] Barry M, Ying J, Durka MJ, Clifford CE, Reddy BVK, Chyu MK. Numerical solution of radiation view factors within a thermoelectric device. Energy 2016;102:427–35.
[60] Zhao D, Tan G. A review of thermoelectric cooling: materials, modeling and applications. Appl Therm Eng 2014;66(1–2):15–24.
[61] Hamid Elsheikh M, Shnawah DA, Sabri MFM, Said SBM, Haji Hassan M, Ali Bashir MB, et al. A review on thermoelectric renewable energy: Principle parameters that affect their performance. Renew Sustain Energy Rev 2014;30:337–55.